High performance piezoelectric MEMS loudspeaker based on an innovative wafer bonding process

Romain Liechti, Stéphane Durand, Thierry Hilt, Fabrice Casset, Christel Dieppedale, Mikael Colin

High performance piezoelectric MEMS loudspeaker based on an innovative wafer bonding process

Romain Liechti [a,b], Stéphane Durand [b], Thierry Hilt [a], Fabrice Casset [a], Christel Dieppedale [a], Mikaël Colin [a]

[a] *Univ. Grenoble Alpes, CEA, Leti, F-38000 Grenoble, France*

[b] *LAUM, Le Mans Université, F-72085 Le Mans, France*

Abstract

Despite a significant number of new structures in the past few years, MEMS loudspeaker still aren't competitive in terms of performance compared to non-MEMS loudspeakers for free field applications. For industrial perspectives, a high sound pressure level on a wide frequency band is required, as well as a low total harmonic distortion. To widen the frequency range of MEMS loudspeakers, we propose to separate the actuating element from the radiating one, in order to separate design constraints to reach an optimal structure. In this paper, the lumped element model of the loudspeaker in presented, as well as the innovative manufacturing process. Finally, the computed frequency response is compared to the measured one. At the resonance, pressures as high as 110 dB_{SPL} at 1 kHz and at 10 mm are reported, which is above the known state of the art for a loudspeaker with similar dimensions. Also, the flatness of the radiated sound pressure in a wide frequency range is closer to the ideal frequency response of loudspeakers than other MEMS loudspeakers, due to the piston mode of the moving rigid plate of the loudspeaker. The total harmonic distortion, mainly due to the nonlinearity of the piezoelectric transduction, is below 5% for reasonable sound pressure levels in the usable frequency band. The use of digital signal processing and of a dedicated packaging will allow our loudspeaker to advantageously replace the main or secondary one in smartphones.

Key words: MEMS; Piezoelectric; Loudspeaker; PZT; Lumped Element; Finite Element.

1 Introduction

A loudspeaker is an electroacoustic transducer, reproducing frequencies in the audio range. More specifically, for full-range loudspeakers, the transducer needs to produce an equal sound pressure level for frequencies from 20 Hz to 20 kHz. Due to several physical limitations, such as the modal behavior of mechanical and acoustical waves, this wide bandwidth is rarely achieved with a single driver in large loudspeaker systems. The acoustic pressure radiated being proportional to the volume of air accelerated by the driver, in the case of a linear actuation, the bandwidth is greatly reduced in the low frequency range, and such loudspeaker are usually reproducing acoustic waves efficiently from 400 Hz to 1 kHz to 20 kHz [1–6]. In the audio chain, the loudspeaker is the last component that is not compatible with the collective manufacturing processes. Despite the effort observed in the past few years, microfabricated loudspeakers performance and footprint are not competitive with those of non-MEMS loudspeakers. For example, the loudspeaker presented in [7] radiates 100 dB_{SPL} at 10 cm at the resonance of 480 Hz and of around 80 dB_{SPL} in a large bandwidth, for a large footprint of more than 1000 mm^2, taking into account the heterogeneously added permanent magnet. The large footprint of this loudspeaker makes it incompatible with modern thin portable devices. The most interesting performance in terms of sound pressure level by unit area are the MEMS loudspeakers actuated by piezoelectric transduction. Some piezoelectric loudspeakers are fully compatible with the microfabrication processes and are showing interesting performance such as the one presented in [8]. Using spin coated sol-gel PZT piezoelectric material, it radiates up to 112 dB_{SPL} at a resonance frequency of 4.2 kHz, for a footprint of 45 mm^2 but the frequency response is affected by the resonance of the membrane, and consequently is far from the ideal desired flat frequency response. Also, the level at frequencies below the first resonance frequency is insufficient and the acoustic pressure was measured using a broadband sound meter, evaluating the harmonic distortion as a part of the radiated sound pressure. In [9] using ZnO as piezoelectric material, a sound pressure level of 76.3 dB_{SPL} at 7.3 kHz for a footprint of 9 mm^2 was reached. The bandwidth and the level are too limited for audio applications, and the frequency response is affected by the modal behavior of the membrane in the

Email address: romain.liechti@cea.fr (Romain Liechti).

audio bandwidth. The device presented in [10] produces a sound pressure level of 108 dB_{SPL} at 8.2 kHz for a footprint of 55 mm^2, but doesn't have a flat frequency response and does not radiate efficiently sound pressure level at lower frequencies. The loudspeaker presented in [11], composed of piezoelectric actuators and a polyimide membrane is radiating about 78 dB_{SPL} at 1 kHz. The frequency response is flat from 500 Hz to 2.5 kHz, but the level is not sufficient for free field applications. Other loudspeakers are actuated using different transductions, such as the one presented in [12] that is built using micromanufacturing techniques and using an electrostatic transduction. It produces a sound pressure level of 50 dB_{SPL} for a footprint of 25 mm^2, but the frequency response is far form the ideal flat spectrum, and the device starts to radiate efficiently acoustics waves only from 8 kHz, which makes it unusable for audio applications. The loudspeaker presented in [13] is an improvement of the loudspeaker presented [8] and shows an increase of the sound pressure level, using a second electrode on the membrane and a phase tuning, but still shows a non-flat frequency response and a too limited sound pressure level. Other loudspeakers, using either electrostatic transduction [14] or thermoacoustic transduction [15] have demonstrated similar frequency responses and low sound pressure level at low frequencies. In terms of mechanical structures, most of these loudspeakers use a deformable membrane, which creates a uneven frequency response. Indeed, deformable membranes should be either highly damped as soft dome loudspeakers, or highly rigid compared to the flexible guiding structure of the loudspeaker, in order to push the first mode of the moving structure outside of the audio bandwidth [16]. Other loudspeakers have been designed for in-ear applications, and are incompatible with the free-field application, due to their high resonance frequency and their small displacement [17–24]. From this overview of recent MEMS loudspeakers, the conclusion is the lack of microfabricated based solution to replace advantageously non-MEMS loudspeaker in portable devices. We present in this paper, the concept, the manufacturing process and the characterization of a new piezoelectric loudspeaker, able to radiate more than 100 dB_{SPL} at 10 mm from 844 Hz to 1492 Hz and a flat frequency response of $98(3)$ dB_{SPL} from 1410 Hz to 7980 Hz. This design is also easily scalable and the dimensions of the moving plate can be reduced, in order to change the resonance frequency for a given application.

2 Results

The loudspeaker concept is presented in Fig. 1. It consists in a pair of piezoelectric bending actuators, arranged symmetrically, and firmly attached to a stiffened plate that can freely moves inside a motionless rigid frame. The bending piezoelectric actuators are composed of a layer of silicon, on which a layer of piezoelectric material is firmly attached between two electrodes. The potential difference between the top and the bottom electrode creates a strain along x into the piezoelectric layer and bends the silicon layer. Due to the symmetry around the z axis, the end of the cantilevers are guided and can only move along z. With an alternative displacement of the plate, surrounding air is accelerated and the displacement of the plate generates an acoustic pressure.

2.1 Theoretical Description

The loudspeaker is designed using a two-port network model with lumped elements assumptions. Similarly to what have been described in [25], an equivalent electrical circuit is determined and depicted in Fig. 2**c**. This electrical equivalent circuit is composed of a serie resistor R_s, representing the electrical resistance of the wires and of the connecting pads, R_p the parallel resistor representing the leaking current path from the top to the bottom electrode of the loudspeaker, C_p the capacitor representing the capacitance created between the top and the bottom electrode, the zener diode representing the breakdown voltage of the piezoelectric layer, γ the linear transduction factor, represented as a transformer and giving the ratio between the voltage u_t to the input force F_{in}. The resistor R_{ms} represents the viscous damping of the resonator, C_{ms} the apparent compliance of the structure and M_{ms} the moving mass of the structure. From the mechanical to the acoustical domain, another transformer is used, with the transduction factor being the surface of the moving rigid plate S_d. The radiation impedance is the one of a square plate and is taken from [26] and represented as the generic impedance Z_{rad}, but can be replaced by the radiation impedance of a circular plate, as they are really similar for a square plate, as it was shown in [25]. The radiation impedance of a circular piston in a infinite baffle is written:

$$Z_{rad} = \rho_0 c_0 S_d \left(1 - \frac{J_1(2ka)}{ka} + j\frac{H_1(2ka)}{ka}\right), \qquad (1)$$

with ρ_0 the air density, c_0 the sound velocity in air, S_d the surface of the piston, a the radius of the piston whose surface is equal to the surface of the square membrane, J_1 the Bessel function of the first order and of the first kind, k the wave number and H_1 the Hankel function of the first kind. The theoretical calculation can be found in [27]. Written as a two-port model, the transfer function can be derived from the schematic using:

$$\begin{bmatrix} u_{in} \\ i_{in} \end{bmatrix} = \begin{bmatrix} 1 & R_s \\ 0 & 1 \end{bmatrix} \begin{bmatrix} 1 & 0 \\ R_p & 1 \end{bmatrix} \begin{bmatrix} 1 & 0 \\ j\omega C_p & 1 \end{bmatrix} \begin{bmatrix} \frac{1}{\gamma} & 0 \\ 0 & \gamma \end{bmatrix} \begin{bmatrix} 1 & R_{ms} \\ 0 & 1 \end{bmatrix} \begin{bmatrix} 1 & j\omega M_{ms} \\ 0 & 1 \end{bmatrix} \begin{bmatrix} 1 & \frac{1}{j\omega C_{ms}} \\ 0 & 1 \end{bmatrix} \begin{bmatrix} S_d & 0 \\ 0 & \frac{1}{S_d} \end{bmatrix} \begin{bmatrix} p_{out} \\ Q_{out} \end{bmatrix}. \qquad (2)$$

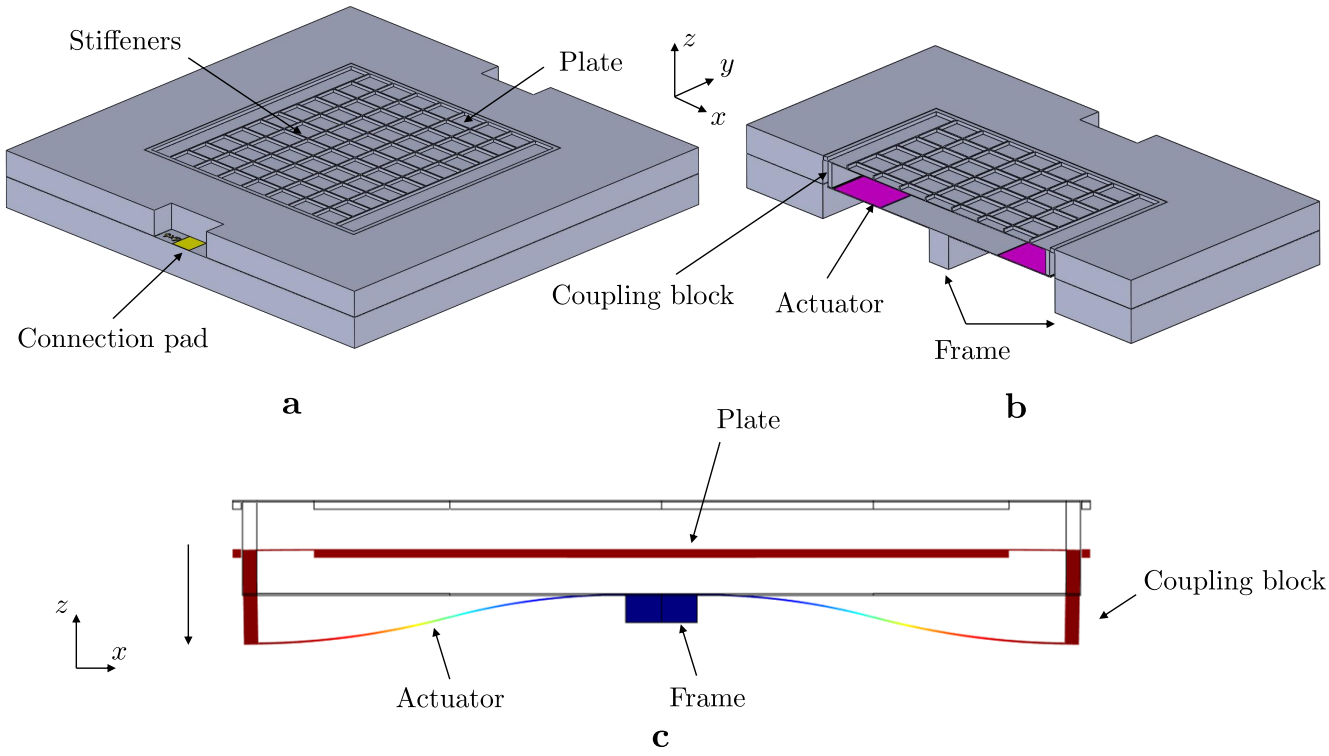

Figure 1. **a** Computer aided drawing of the designed loudspeaker showing the two wafers configuration and the stiffened plate, as well as one of the connection pad on the top of the bottom wafer. **b** Cut view of the computer aided drawing of the loudspeaker, displaying the actuators and the center frame, as well as the coupling blocks. **c** cut view of the designed loudspeaker in Comsol Mulitphysics, showing the clamped-guided deformation profile of the actuators, and the translation of the rigid plate in the top wafer.

By multiplying the matrices together, equation 2 reduces to:

$$\begin{bmatrix} u_{in} \\ i_{in} \end{bmatrix} = \begin{bmatrix} A & B \\ C & D \end{bmatrix} \begin{bmatrix} p_{out} \\ Q_{out} \end{bmatrix}, \tag{3}$$

and adding the radiation impedance at the output of the equivalent quadripole, depicted in Fig. 2**e**, the output volume velocity Q_{out} can be expressed as

$$Q_{out} = \frac{u_{in}}{A + \frac{B}{\Re(Z_{rad})}}. \tag{4}$$

Using the plane waves assumption and a simple tube model, represented in Fig. 2**d**, the back impedance of the loudspeaker, composed of short sections of rectangular ducts with different surfaces, can be approximated with a lossy tube model

$$\begin{bmatrix} p_{in} \\ Q_{in} \end{bmatrix} = \begin{bmatrix} cos(k_c L) & jZ_c sin(k_c L) \\ \frac{j}{Z_c} sin(k_c L) & cos(k_c L) \end{bmatrix} \begin{bmatrix} p_{out} \\ Q_{out} \end{bmatrix}. \tag{5}$$

The total impedance, seen by the moving plate is then derived as the ratio between the input pressure p_{in} over the input volume velocity Q_{in} and is written

$$Z_b = \frac{A_b Z_{rb} + B_b}{C_b Z_{rb} + D_b} \tag{6}$$

Z_{rb} being the radiation impedance of the last rectangular portion of the loudspeaker, assumed to be equal to the radiation impedance of a rigid piston in an infinite baffle of the same dimensions as the rectangular opening. From the geometrical simplification of the problem shown in Fig. 2**a**, describing a rectangular surface S_d vibrating harmonically with a velocity v, along an axis z, normal to the surface and flush mounted in an infinite baffle the pressure generated by the surface as a function of the elevation angle ϕ, the azimuth angle θ and the distance **r** can be expressed as

$$p(r,\theta,\phi,\omega) = -j\rho_0 c_0 Q_{out} \frac{\sin\frac{\theta a}{2}\sin\frac{\phi b}{2}}{\theta\phi ab} \frac{e^{jk_0 r}}{2\pi r}. \tag{7}$$

The biggest dimension of the plate being small against the wavelength of the highest audio frequency, the loudspeaker is theoretically omnidirectionnal in the audio bandwidth, as it is shown in Fig. 2**b** for four frequencies. Similarly to

equation 6, the electrical impedance Z_e of the loudspeaker can be derived using the complete equivalent circuit depicted in Fig. 2**c**

$$Z_e = \frac{u_{in}}{i_{in}} = \frac{AZ_a + B}{CZ_a + D}, \tag{8}$$

Z_a being the complete acoustical impedance seen by the loudspeaker from the mechanical domain through the surface S_d.

2.2 Loudspeaker Design

Using the circuit described in Fig. 2**c**, the loudspeaker is optimized by choosing the surface of the plate and the thickness of the elastic layer of the actuators to determine the frequency response of the loudspeaker. These parameters are chosen in order to keep the surface of the loudspeaker under 100 mm^2 in order to be placed advantageously under the usual footprint of 11×15 mm^2 of classical non-MEMS loudspeakers. The target resonance frequency is set around 1 kHz with a radiated sound pressure level of approximately 80 $\mathrm{dB_{SPL}}$ in the bandwidth. Using the finite element model described in [25], the modal behavior of the loudspeaker was optimized by choosing the number of the stiffeners of the plate, in order to push the first eigenmode of the plate higher in frequency, and to keep the mass of the plate low enough hence avoiding to alter the sensitivity. Main lumped element equivalent parameters of the loudspeaker are recalled in Table 1.

2.3 Manufacturing Process

The loudspeaker is manufactured out of 200 mm silicon wafers using the process detailed in Fig. 3. Starting from two SOI wafers whose first wafer has a handle wafer thickness of 675 µm and a device layer of 12 µm and whose second wafer has a handle wafer of 500 µm and a device layer of 80 µm. A layer of PZT is then deposited by spin coating on a hardened oxide and on a platinum bottom electrode on the device layer of the first wafer, after having patterned a hard mask on the handle wafer side. A top electrode is then deposited and etched and is then protected by a passivation layer, etched only locally to open pads on the bottom and top electrodes. An etching is then performed around the actuators in the device layer, as a pre-release. The glue is then deposited and patterned, on the frame and on the ends of the actuators (Fig. 3**a**). The second wafer is completely etched with a DRIE on the handle wafer side, after a hard mask was deposited and etched and a partial etch was performed on the device layer side (Fig. 3**b**). Both wafers are then glued together in a partial vacuum (Fig. 3**c**). The second part of the partial etch on the device layer side of the second wafer is then performed to obtain the finished rigid plate. The final released is then performed by a deep etching of the handle wafer side of the first wafer. The remaining oxides of the BESOI wafers are then removed with a plasma etching at the end of the process (Fig. 3**d**).

In Fig. 4, a few pictures of the manufactured loudspeakers are presented. Fig. 4**a** depicts a SEM cross section of one of the actuators, highlighting the typical slope after etching the PZT layer and the silicon thickness of the elastic part of the actuator. A zoom on the PZT layer is depicted in Fig. 4**b** on which the bottom and the top platinum electrodes are visible. In Fig. 4**c** a cross section SEM view of the plate shows the partial etching of a stiffener. Fig. 4**d** depicts an infrared view of both wafers after the alignment process, before the bonding step. Fig. 4**e** and 4**f** show the front and the back of the loudspeaker after the final release etching.

2.4 Measurement Setup and Results

In Fig. 5**a** the crystalline orientation of the piezoelectric material measured using a Bruker XRD3 is presented. The count per second as a function of the angle shows the required main orientation of the PZT 100 at 21.9°, and two orders of magnitude lower, the orientation 110 at 31.3°. The third peak at an angle of 38.2° is due to the orientation 111 and the last peak at 40° is due to the platinum electrodes, above and below the piezoelectric layer. In Fig. 5**b**, the P-E hysteresis curve, measured using a AixACCT TF Analyzer 2000 is presented. It evidences the usual lossy but linear hysteresis for a low electric field of 25 kV m^{-1} and it shows the usual nonlinear hysteresis ferroelectric loop, with a polarization voltage above 25 V. The electro-mechanical coefficient is estimated using a aixDBLI and presented in Fig. 5**c**. The measurement is performed by measuring the displacement on wafer using a laser interferometer. The measurement is smoothed and at amplitudes of 30 V and 50 V the typical butterfly loop is clearly identifiable, confirming the usual ferroelectric behavior of the thin film PZT. From the built-in model of the analyzer, the parameter $e_{31,f}$ is estimated to be between 15 and 17 C m^{-2} between 20 and 30 V. In Fig. 5**d** the absolute value of the electrical impedance of the loudspeaker, measured using a E4990A Impedance Analyzer is shown and compared to equation 8 and the value of C_p is adjusted to 70 nF to fit the measurement. The values of R_p and R_s are respectively too large and too small to be determined using the impedance measurement in the audio range and can be neglected. Slightly above 1 kHz, the effect of the mechanical resonance of the loudspeaker is observed on the measurement and corresponds to the one simulated with the two port network. As the amplifier is a voltage amplifier, the voltage u_{in} can be considered constant in the audio bandwidth, and the current as a function of frequency can be calculated, in order to derive the sensitivity of the loudspeaker.

In order to be characterized acoustically, the loudspeaker is mounted on a custom printed circuit board, depicted in Fig. 6**a**. To avoid an acoustics short-cut in the lower frequency range and to avoid change the back acoustic load of the loudspeaker, the printed circuit board is mounted on a

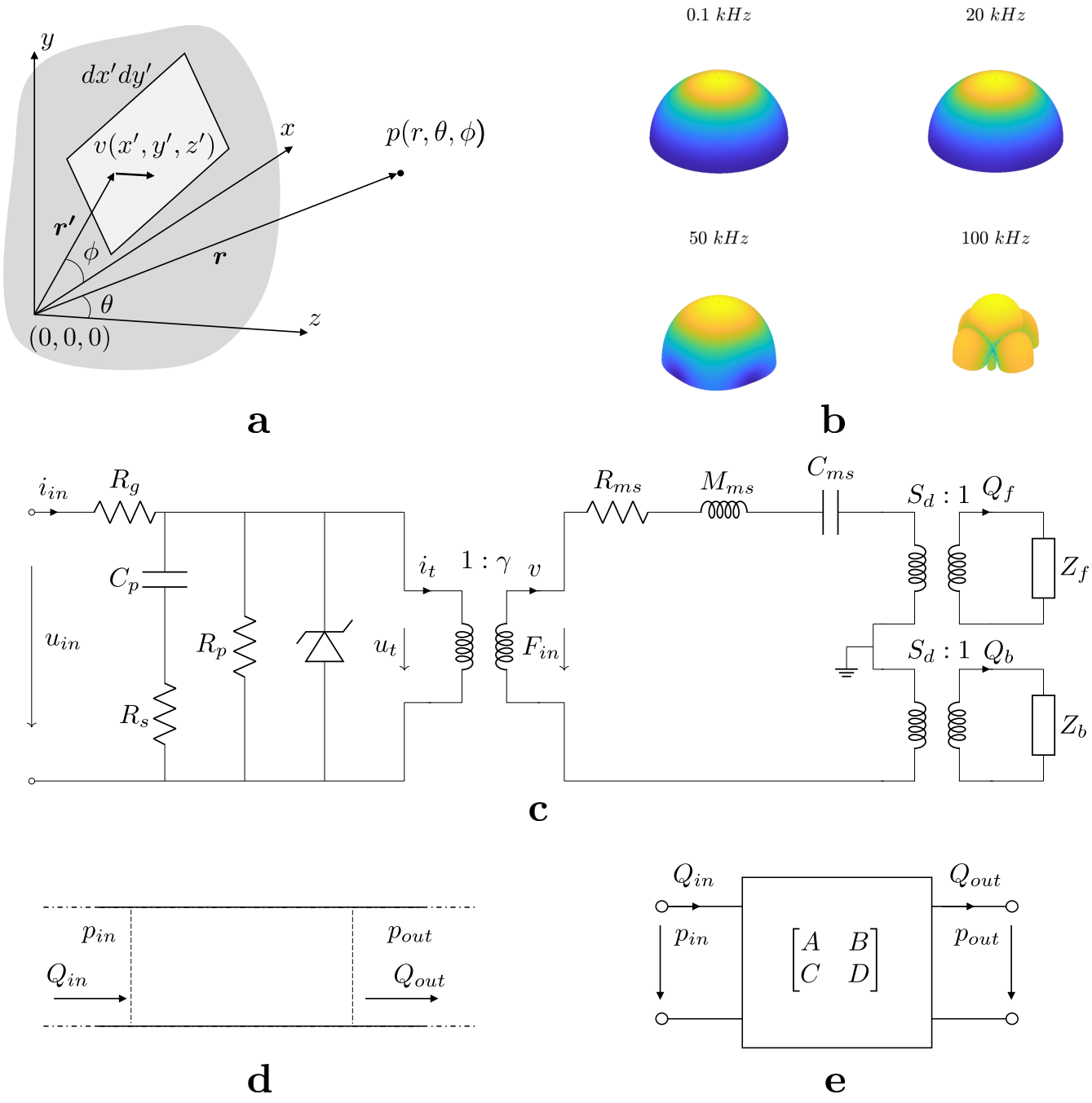

Figure 2. **a** Schematic of a rigid rectangular piston vibrating in a infinite baffle with the relevant angles and distance, defining the position of evaluation of the pressure and **b** visualization of the directivity, calculated using equation 7, for four frequencies in the audio and ultrasonic range. **c** equivalent electrical circuit of the designed loudspeaker. **d** schematic of a tube in the plane wave assumption with the input and output pressure p_{in} and p_{out} and the input and output volume velocity Q_{in} and Q_{out}. **e** quadripole representing the equivalent transfer function of a tube assuming plane waves, whose frequency dependent coefficients A, B, C and D are linking the input volume velocity and pressure to the output volume velocity and pressure.

$200 \times 200\,\mathrm{mm}^2$ aluminum rigid baffle (Fig. 6**c**). The loudspeaker is then measured using the measurement setup depicted in Fig. 6**d**. Fig. 6**c** shows a picture of the setup. A sine sweep signal is generated using LABView on the computer mounted in the same chassis as the PXI 4461 acquisition card. The microphone signal is amplified by the G.R.A.S. 12AL and sampled at 192 kHz by the acquisition card. A reference level is measured using a GRAS 42AG multifunc-

Parameter	Value	Unit
C_p	$18 \cdot 10^{-8}$	F
γ	0.48	$\mathrm{mN\,V^{-1}}$
R_{ms}	$4 \cdot 10^{-6}$	$\mathrm{N\,s\,m^{-1}}$
M_{ms}	$5.8 \cdot 10^{-6}$	kg
C_{ms}	$11 \cdot 10^{-3}$	$\mathrm{m\,N^{-1}}$
S_d	$64 \cdot 10^{-6}$	$\mathrm{m^2}$

Table 1
Lumped elements parameters of the loudspeaker

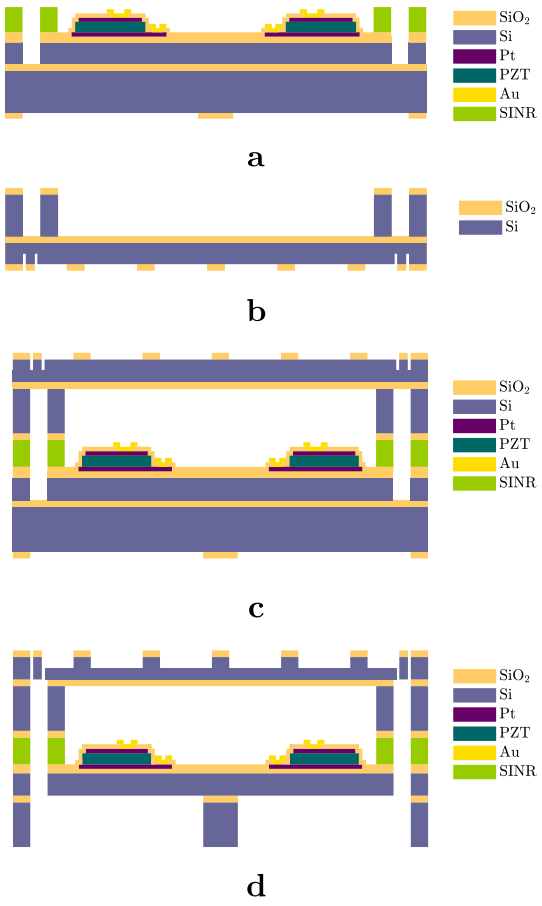

Figure 3. **a** Last step of the first wafer processing, after depositing and etching the SINR. **b** Last step of the second wafer processing, after the deep etching of the back cavity. **c** Assembly of the top wafer over the bottom wafer. **d** finished loudspeaker, after the back deep etching and the etching of the remaining oxides layers.

tion sound calibrator at different frequencies and levels.

The loudspeaker is actuated by a custom DC coupled amplifier, providing a DC voltage of 14.5 V and a gain of 15, as depicted in Fig. 7**a**, for an input voltage of 100 mV at 1 kHz. The measured frequency response is presented in Fig. 7**b** and is in agreement with the model on a large bandwidth, below and above the first resonance of the loudspeaker. Considering uncertainties due to the manufacturing process and the measurement setup, a upper and lower bounds are calculated using the propagation of uncertainties. The value of the viscous damping R_{ms} is adjusted to fit the measurement, to a value of $6\,\mathrm{mN\,s\,m^{-1}}$, as this parameter is difficult to predict, due to the complexity of the multiple sources of damping. At this amplitude, the viscous damping might differ from the value determined at lower actuation voltages, due

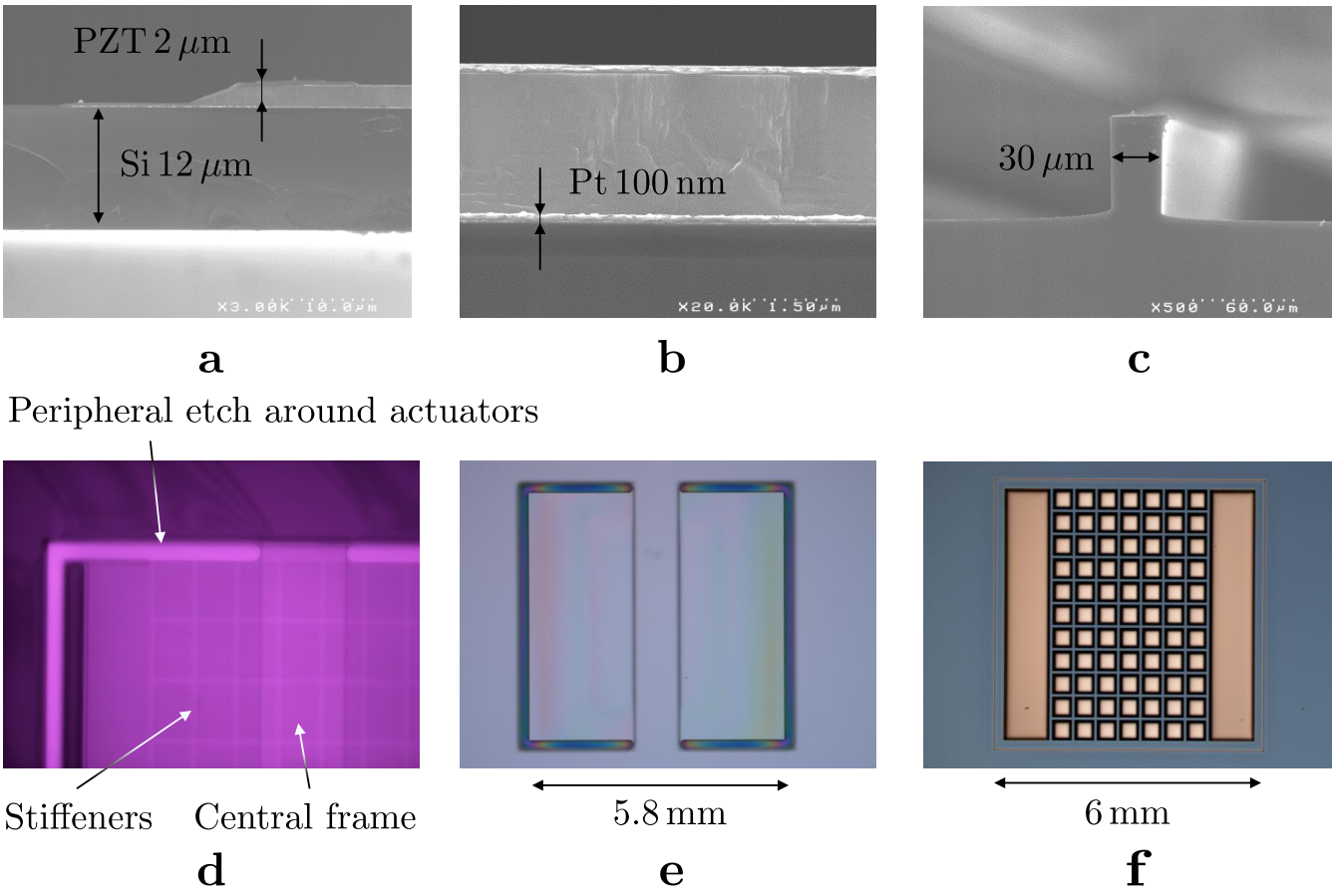

Figure 4. **a** SEM cross section view of the actuator. **b** SEM cross section view of the piezoelectric layer between the two platinum electrodes. **c** SEM crosse section view after the partial etch of one of the stiffeners. **d** infrared microscope view of both wafers. **e** back microscope view of the loudspeaker after the final release. **f** front view of the loudspeaker after release.

to geometrical nonlinearities compressing the displacement at the resonance. The measured frequency response is within the bounds from 200 Hz to 5 kHz. The first peak at approximately 9 kHz is due to the second mode of the actuators, followed by the complex modal behavior of the plate, leading to a non-flat response above 7 kHz. This could be corrected easily with a digital signal processing chipset, as the measurement on wafer has shown a small standard deviation from a loudspeaker to another. As predicted by the theoretical model and as it is presented in Fig. 7**c**, the loudspeaker is not directive in the audio bandwidth. The total harmonic distortion measured at an actuation voltage of 15 V_{AC}+1.5 V_{DC} and depicted in Fig. 7**d** is below 5% for most of the usable frequency range. A net increase of the THD is observed at half and a third of the resonance frequency, due to the linear amplification of the second and third harmonics at these frequencies. An increase of the distortion at the resonance of the loudspeaker, slightly above 1 kHz, is also observed as the displacement is out of the mechanical linear range of the loudspeaker. These peaks of distortion could be corrected by damping mechanically or electronically the resonance of the loudspeaker. Below the peaks, the THD increases below the resonance frequency of the loudspeaker, as the displacement in this frequency range is maximum. The distortion becomes high from 4 kHz, where the modal behavior of the plate amplifies the harmonics and is not shown here. These problems could be solved by linearly decreasing the peaks of the frequency response with digital notch filters for example.

3 Conclusion

A high performance MEMS loudspeaker was designed using analytical calculations as well as finite element modeling, and built using an innovative two silicon wafers process. The lumped element model accurately predicted the radiated sound pressure level and the resonance frequency of the loudspeaker around the resonance. Performance of the loudspeaker is above the known perfomance of MEMS loudspeakers of similar dimensions, in terms of sound pressure level, bandwidth and total harmonic distortion. Using a dedicated packaging with an additional acoustical bandpass filter, and digital signal processing to correct the frequency response, this loudspeaker could replace non-MEMS loudspeakers in some portable devices, performance wise, as a few more dB can be expected with the correct packaging and

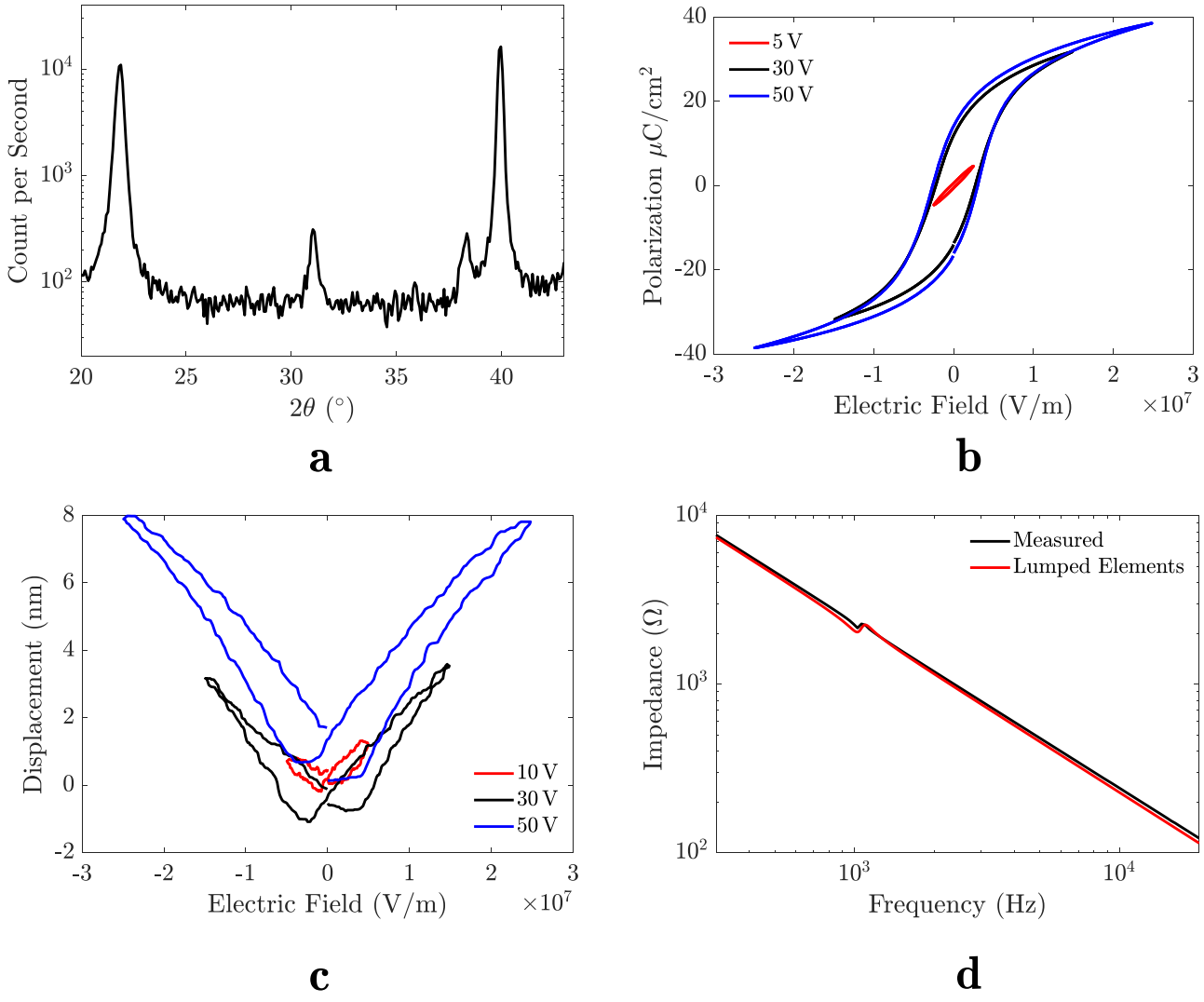

Figure 5. **a** XRD measurement of the crystalline orientation of the PZT showing the desired orientation of the PZT at $2\theta = 100$. **b** P-E hysteresis loop of the manufactured PZT measured after the etching of the electric contacts on the devices. **c** piezoelectric measurement of the manufactured piezoelectric material on devices. **d** electrical impedance of the loudspeaker measured using a E4990A Impedance Analyzer and compared to the one calculated using the two port equivalent model.

signal processing. The small form factor and especially the thickness of 1.2 mm could allow to use multiple loudspeakers to reach even higher performances in terms of radiated sound pressure. Also, the design being composed of actuators using only approximately half of the deformable silicon layer, the other half could be used for an integrated sensor in order to implement active control on the loudspeaker, to improve the frequency response and reduce the total harmonic distortion. It could also be used passively with a resistor to reduce the quality factor of the first resonance. This proof of concept also shows that the designed loudspeaker can withstand larger displacements and so it means that the actuation could be higher that 30 V in the bandwidth, in order to reach higher sound pressure level, with the adequate digital signal processing or damping at the first resonance.

4 Acknowledgments

We would like to thank the Carnot Institute for the funding for this research.

References

[1] Chang-Min Lee, Joong-Hak Kwon, Kwang-Suk Kim, Jin-Hun Park, and Sang-Moon Hwang. Design and analysis of microspeakers to improve sound characteristics in a low frequency range. *IEEE Transactions on Magnetics*, 46(6):2048–2051, 2010.

[2] Sang-Moon Hwang, Hong-Joo Lee, Ji-Hoon Kim, Joong-Hak Kwon, Kuem-Shik Hong, and Gun-Yong Hwang. Development of hi-fi microspeakers with a woofer and a tweeter used for mobile phones. *Journal of applied physics*, 97(10):10R512, 2005.

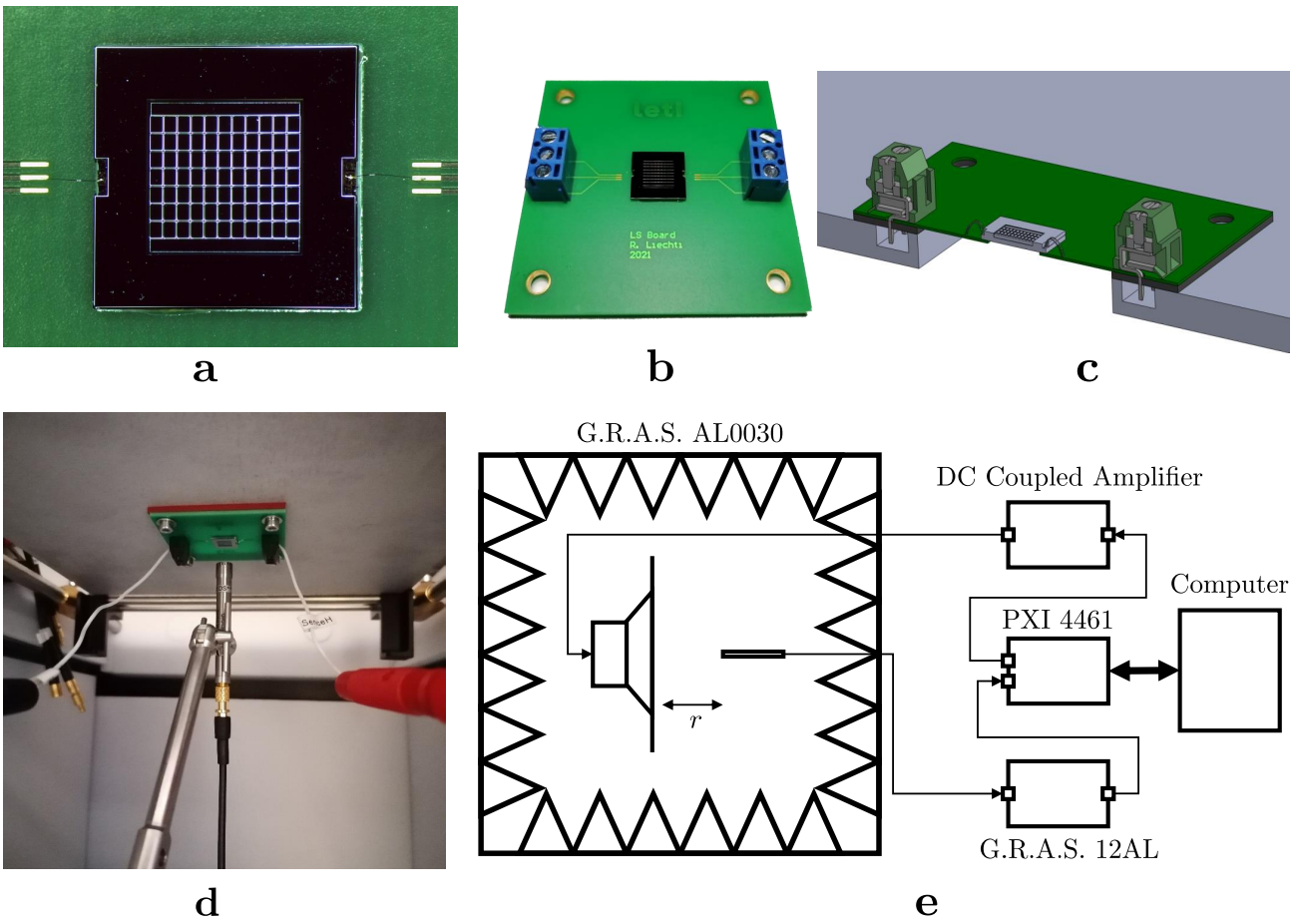

Figure 6. **a** picture of the loudspeaker mounted on a custom PCB. **b** picture of the loudspeaker mounted on the custom PCB board. **c** CAD cut view of the loudspeaker mounted on the printed circuit board, on the $200 \times 200\,\mathrm{mm}^2$ baffle. **d** picture of the loudspeaker mounted on the printed circuit board and on the baffle in the anechoic box. **e** measurement setup composed of an anechoic chamber, simulating a free field environment, an NI acquisition card, a G.R.A.S. 46 BE microphone, a G.R.A.S. microphone power supply and amplifier, and a DC coupled amplifier.

[3] Joong-Hak Kwon, Sang-Moon Hwang, and Kwang-Seok Kim. Development of slim rectangular microspeaker used for minimultimedia phones. *IEEE Transactions on Magnetics*, 43(6):2704–2706, 2007.

[4] Yusuke Nakashima, Tomoyuki Ohya, and Takeshi Yoshimura. Prototype of parametric array loudspeaker on mobile phone and its acoustical characteristics. In *Audio Engineering Society Convention 118*. Audio Engineering Society, 2005.

[5] Toshiyuki Matsumura, Shuji Saiki, Koji Sano, and Sawako Usuki. Ultra-thin micro-loudspeaker using oblique magnetic circuit. In *Audio Engineering Society Convention 124*. Audio Engineering Society, 2008.

[6] Jin H Huang, Hong-Ching Her, YC Shiah, and Shaw-Jyh Shin. Electroacoustic simulation and experiment on a miniature loudspeaker for cellular phones. *Journal of Applied Physics*, 103(3):033502, 2008.

[7] Iman Shahosseini, Elie Lefeuvre, Johan Moulin, Emile Martincic, Marion Woytasik, and Guy Lemarquand. Optimization and microfabrication of high performance silicon-based mems microspeaker. *IEEE Sensors Journal*, 13(1):273–284, 2012.

[8] Haoran Wang, Zhenfang Chen, and Huikai Xie. A high-spl piezoelectric mems loud speaker based on thin ceramic pzt. *Sensors and Actuators A: Physical*, 309:112018, 2020.

[9] Sang Choon Ko, Yong Chul Kim, Seung Seob Lee, Seung Ho Choi, and Sang Ryong Kim. Micromachined piezoelectric membrane acoustic device. *Sensors and Actuators A: Physical*, 103(1-2):130–134, 2003.

[10] Haoran Wang, Mengyuan Li, Yuanyuan Yu, Zhenfang Chen, Yingtao Ding, Huabei Jiang, and Huikai Xie. A piezoelectric mems loud speaker based on ceramic pzt. In *2019 20th International Conference on Solid-State Sensors, Actuators and Microsystems & Eurosensors XXXIII (TRANSDUCERS & EUROSENSORS XXXIII)*, pages 857–860. IEEE, 2019.

[11] Il-Joo Cho, Seongsoo Jang, and Hyo-Jin Nam. A piezoelectrically actuated mems speaker with polyimide membrane and thin film pb (zr, ti) o3 (pzt) actuator. *Integrated Ferroelectrics*, 105(1):27–36, 2009.

[12] Hanseup Kim, Aaron A Astle, Khalil Najafi, Luis P Bernal, Peter D Washabaugh, and Fernando Cheng. Bi-directional electrostatic microspeaker with two large-deflection flexible membranes actuated by single/dual electrodes. In *SENSORS, 2005 IEEE*, pages 4–pp. IEEE, 2005.

[13] Haoran Wang, Philip X-L Feng, and Huikai Xie. A dual-electrode mems speaker based on ceramic pzt with improved sound pressure

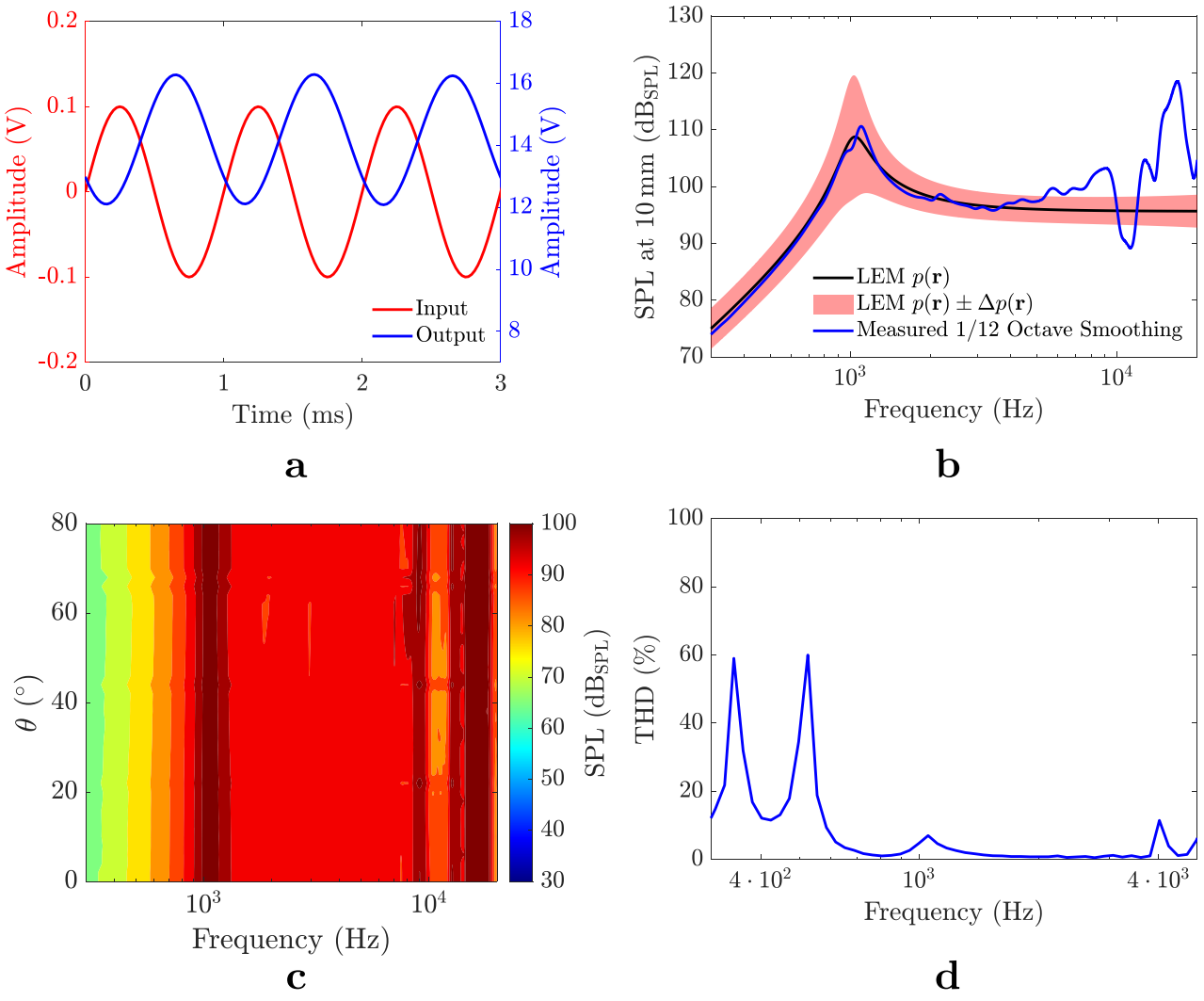

Figure 7. **a** input and output signal of the custom amplifier used to actuate the loudspeaker. **b** frequency response of the loudspeaker actuated at 15 V_{AC}+15 V_{DC} compared to the frequency response calculated using the two port model. **c** directivity of the loudspeaker measured every 2° on a range of 90° from the normal axis to the perpendicular axis of the loudspeaker. **d** total harmonic distortion of the loudspeaker actuated at 15 V_{AC}+1.5 V_{DC}, corresponding to a level of 96.5 dB_{SPL} at 1 kHz and at a distance of 10 mm

level by phase tuning. In *2021 IEEE 34th International Conference on Micro Electro Mechanical Systems (MEMS)*, pages 701–704. IEEE, 2021.

[14] Robert C Roberts, Jiangang Du, Andojo Ongkodjojo Ong, Dachao Li, Christian A Zorman, and Norman C Tien. Electrostatically driven touch-mode poly-sic microspeaker. In *SENSORS, 2007 IEEE*, pages 284–287. IEEE, 2007.

[15] He Tian, Yi Yang, Dan Xie, Tian-Ling Ren, Yi Shu, Chang-Jian Zhou, Lu-Qi Tao, and Li-Tian Liu. Flexible and large-area sound-emitting device using reduced graphene oxide. In *2013 IEEE 26th International Conference on Micro Electro Mechanical Systems (MEMS)*, pages 709–712. IEEE, 2013.

[16] John Eargle. *Loudspeaker handbook*. Springer Science & Business Media, 2003.

[17] Bert Kaiser, Sergiu Langa, Lutz Ehrig, Michael Stolz, Hermann Schenk, Holger Conrad, Harald Schenk, Klaus Schimmanz, and David Schuffenhauer. Concept and proof for an all-silicon mems micro speaker utilizing air chambers. *Microsystems & Nanoengineering*, 5(1):1–11, 2019.

[18] Fabian Stoppel, Andreas Männchen, Florian Niekiel, Daniel Beer, Thorsten Giese, and Bernhard Wagner. New integrated full-range mems speaker for in-ear applications. In *2018 IEEE Micro Electro Mechanical Systems (MEMS)*, pages 1068–1071. IEEE, 2018.

[19] Markus Hänsler, Giacomo Muraro, Christian Novotny, Richard Murphy, Jakob Spötl, and Andrea Rusconi Clerici. Mems based audio speaker module. In *Audio Engineering Society Convention 148*. Audio Engineering Society, 2020.

[20] Hsu-Hsiang Cheng, Sung-Cheng Lo, Zi-Rong Huang, Yi-Jia Wang, Mingching Wu, and Weileun Fang. On the design of piezoelectric mems microspeaker for the sound pressure level enhancement.

Sensors and Actuators A: Physical, 306:111960, 2020.

[21] Ahmed Fawzy, Yiming Lang, and Menglun Zhang. Design and analysis of piezoelectric mems micro-speaker based on scandium-doped aln thin film. *Micro & Nano Letters*, 16(3):227–231, 2021.

[22] Ming-Cheng Cheng, Wen-Sheh Huang, and Star Ruey-Shing Huang. A silicon microspeaker for hearing instruments. *Journal of Micromechanics and Microengineering*, 14(7):859, 2004.

[23] Sang-Soo Je, Fernando Rivas, Rodolfo E Diaz, Jiuk Kwon, Jeonghwan Kim, Bertan Bakkaloglu, Sayfe Kiaei, and Junseok Chae. A compact and low-cost mems loudspeaker for digital hearing aids. *IEEE Transactions on Biomedical Circuits and Systems*, 3(5):348–358, 2009.

[24] Yu-Tzu Lin, Sung-Cheng Lo, and Weileun Fang. Two-way piezoelectric mems microspeaker with novel structure and electrode design for bandwidth enhancement. In *2021 21st International Conference on Solid-State Sensors, Actuators and Microsystems (Transducers)*, pages 230–233. IEEE, 2021.

[25] Romain Liechti, Stéphane Durand, Thierry Hilt, Fabrice Casset, Christel Dieppedale, Thierry Verdot, and Mikaël Colin. A piezoelectric mems loudspeaker lumped and fem models. In *2021 22nd International Conference on Thermal, Mechanical and Multi-Physics Simulation and Experiments in Microelectronics and Microsystems (EuroSimE)*, pages 1–8. IEEE, 2021.

[26] Fridolin P Mechel. Formulas of acoustics, 2004.

[27] Philip McCord Morse and K Uno Ingard. *Theoretical acoustics*. Princeton university press, 1986.